Band structure and its temperature dependence for type-III HgTe/$Hg_{1-x}Cd_xTe$ superlattices and their semimetal constituent

C. R. Becker,* V. Latussek, A. Pfeuffer-Jeschke, G. Landwehr, and L. W. Molenkamp
Physikalisches Institut der Universität Würzburg, Am Hubland, 97074 Würzburg, Germany
(Received 15 March 2000)

Intersubband transitions in HgTe/$Hg_{1-x}Cd_xTe$ superlattices and their dependence on temperature have been investigated for a large number of superlattices with widely different parameters. It has been shown by means of the envelope function approximation using the full 8×8 Kane Hamiltonian, that the valence band offset is primarily responsible for the separation between the $H1$-$E1$ and $L1$-$E1$ intersubband transition energies of semiconducting HgTe/$Hg_{1-x}Cd_xTe$ superlattices with a normal band structure. To a good approximation, all other relevant superlattice parameters have little or no effect on this energy difference. This leads to an unequivocal determination of the valence band offset between HgTe and CdTe Λ which is 570 ± 60 meV at 5 K for both the (001) and the (112)B orientations. The temperature dependence of both intersubband transition energies can only be explained by the following conditions: Λ is also temperature dependent as expressed by $d\Lambda/dT=-0.40\pm0.04$ meV/K; the anisotropic heavy hole effective mass has a significant temperature dependence; and $E_g(\mathrm{HgTe,300\ K})=-160\pm5$ meV which is appreciably lower than the extrapolated values found in the literature.

I. INTRODUCTION

The band structure of type-III superlattices (SL's) and their related properties are largely determined by that of the quantum well. Conversely, an investigation of the optical and electrical properties of type-III superlattices can lead to information about the zero gap or semimetallic material used in the quantum well. Hence one has the unique opportunity to investigate properties of the semimetal which cannot easily be investigated by other methods.

For example, the band gap of HgTe and its temperature dependence directly influences the temperature dependence of the superlattice subbands and thus the temperature dependence of the intersubband transition energies. The magnitude of the negative band gap of HgTe at room temperature is subject to large experimental uncertainties due to difficulties in the conventional magneto-optical method at temperatures above 100 K.[1] Another such property is the deformation potential of HgTe relative to that of CdTe, which has only recently been experimentally determined by means of an optical absorption investigation of HgTe/$Hg_{0.32}Cd_{0.68}Te$ superlattices under hydrostatic pressure.[2] Furthermore, it will be shown that the valence-band offset is to a good approximation primarily responsible for the energy difference between the first heavy-hole $H1$ and the first light-hole $L1$ subband of a HgTe/$Hg_{1-x}Cd_xTe$ superlattice with normal band structure. This energy difference is nearly independent of other superlattice parameters, and consequently leads to a precise determination of the valence-band offset between HgTe and CdTe Λ.

The band structure and consequently the optical properties depend on the band structure of the quantum wells and barriers, i.e., HgTe and $Hg_{1-x}Cd_xTe$, their widths, and the potential energy differences between these two components. The latter depends in turn on their composition, the valence-band offset as well as the shape and width of the Cd concentration profile across the interfaces. A profile described by an error function similar to an experimental profile according to Kim *et al.*[3] is assumed and leads to a consistent description of the experimental results. Finally, the width of this interface, d_t, has been shown to be a convenient variable for the study of interdiffusion in these superlattices.[4]

In order to accomplish the above, one has to determine the relevant experimental intersubband transition energies. However, this is not a trivial undertaking due, to a large extent, to a lack of knowledge about the position of a particular band gap relative to the frequency of photoluminescence peaks,[5–7] or that of the absorption edges.[8] The method we propose and demonstrate here, is to determine the position of the absorption edge and then its position relative to the intersubband transition energy itself. This can be accomplished by calculating the transition energies as well as the corresponding absorption coefficient. Finally, by fitting the theoretical and experimental absorption coefficients, one can determine the experimental intersubband transition energies relative to their absorption edges.

II. EXPERIMENTAL DETAILS

Epitaxial growth was carried out in a Riber 2300, molecular beam epitaxial system that has been modified to permit the growth of Hg-based materials as has been described elsewhere.[4] After the growth of a thin CdTe buffer layer, the HgTe/$Hg_{1-x}Cd_xTe$ superlattices were grown on (001) and (112)B oriented $Cd_{0.96}Zn_{0.04}Te$ and CdTe substrates at 180 °C with the exception of three (112)B SL's at 188 °C. The substrate temperature was determined with an accuracy of $\pm$ 2 °C by means of a thermocouple which was in physical contact with a molybdenum substrate holder. The thermocouple was carefully calibrated at the melting points of indium and tin.

The composition of the barrier material has been determined by means of transmission measurements[9] on thick test

layers of $Hg_{1-x}Cd_xTe$ grown under identical conditions with the exception of the absence of the HgTe layers. At a growth temperature of 180 °C, $x=0.68\pm0.02$ and $x=0.95\pm0.02$ for the (001) and (112)B orientations, respectively. This value has been corroborated by a determination of the barrier TO phonon frequency for several (001) SL's.[10] Cd has been found in some thin layers of HgTe grown under similar conditions by means of *in situ* x-ray photoelectron spectroscopy. If the Cd is evenly distributed throughout the layer then an average concentration in the well x_w can be calculated. Usually this value was below the sensitivity of the spectrometer, i.e., much less than 0.5%, however, 3.0% was determined on one occasion. The latter value was shown to be due to sublimation from the hot CdTe shutter, which depends on what was grown previously. Nonlinear diffusion[11] may also account for the presence of small amounts of Cd in the HgTe wells.

The superlattice period is readily accessible by x-ray diffraction experiments; however well and barrier thicknesses are not so easily determined. Historically well and barrier thicknesses have been inferred from the growth parameters, measured by transmission electron microscopy[12] or determined by means of a simulation of high resolution x-ray diffraction results.[13,14] In this investigation we have determined the well thickness and hence that of the barrier of (001) superlattices via a dynamic simulation of the (002) and (004) Bragg reflections measured in a five crystal x-ray diffractometer. The rather strong (002) Bragg reflection in these superlattices is caused primarily by the HgTe layer: The structure factor for the (002) Bragg reflection is much larger for HgTe than for CdTe.[13] This is due to the larger Hg atom with its greater number of electrons. In fact the structure factor goes to zero for $Hg_{1-x}Cd_xTe$ with an x value of about 0.88. A simulation of (001) oriented superlattices results in an accuracy as low as $\pm$ 1 Å but which is usually ± 2 Å, depending on the number of satellites and the position of the first order zero points relative to the satellites.

X-ray diffraction in $(112)B$ oriented heterostructures is more complicated and the results less accurate. First of all, there is only one useful reflection (224) which is not stronger for either HgTe or CdTe. Second, shear strain results in a monoclinic distortion which must be taken into account before the data can be correctly simulated.[15,16]

Optical transmission and reflection measurements were carried out in the middle and near infrared with a Fourier transform spectrometer, Bruker IFS88. A $LiTaO_3$ detector was usually employed rather than a liquid nitrogen cooled detector, e.g., $Hg_{1-x}Cd_xTe$, because of its better linearity. The aperature was kept as small as possible for the same reason, i.e., a diameter of 2–3 mm. The absorption coefficient was determined by fitting the experimental transmission spectra to a theoretical description of the multilayer system using standard matrix procedures.[17]

It can be easily shown that a transmission spectrum divided by a slightly different spectrum, e.g., measured at a different temperature, is proportional to the corresponding change in the absorption coefficient

$$\frac{\Delta T}{T}=\frac{T_2}{T_1}-1\approx d\Delta\alpha, \tag{1}$$

where T and d are the transmission and sample thickness, respectively. Hence a good approximation of $\Delta\alpha$, see Fig. 4, can be obtained merely from a ratio of the transmission spectra without the complications and uncertainties in calculating the absorption spectrum of the SL in a multilayer structure.[17] If the temperature difference is kept small, $\Delta T=20-40$ K, residual interference effects can be effectively reduced near the transition itself and nearly elliminated at other frequencies. The index of refraction n undergoes a change of up to about 5%–10% near an intersubband transition, however, this has been shown to result in a negligible shift of the experimental absorption edge of $\leqslant 1$ meV.

The transmission spectra of most of the SL's were measured at various temperatures. In most cases this was done from 5 to 300 K with a temperature interval of 10 K, in order to improve the statistical significance of the data.

III. THEORETICAL DETAILS

A large number of $\mathbf{k}\cdot\mathbf{p}$ band structure calculations using the envelope function approximation for the $HgTe/Hg_{1-x}Cd_xTe$ superlattice have been published during the last decade.[18–21] Wood and Zunger[22] have compared the predictions of a pseudopotential approach, which includes all bands and their dispersion throughout the Brillouin zone and produces wave functions with full Bloch symmetry, with predictions of an 8×8 multiband $\mathbf{k}\cdot\mathbf{p}$ approach in the envelope function approximation. The authors conclude that the latter model works well for heterostructures when their states are derived from bulk states which are *well* described by $\mathbf{k}\cdot\mathbf{p}$, i.e., from states near the Γ point. Ram-Mohan, Yoo, and Aggarwal[18] employed the envelope function method and developed a transfer matrix procedure to calculate the superlattice states. They accounted for the full 8×8 Kane Hamiltonian including all second order terms representing the far-band contributions, but did not apply their results to a calculation of the optical constants. On the other hand Johnson *et al.*[19] applied a slightly different version of the envelope function method, and deduced optical constants from their superlattice energies and eigenfunctions. But in their approach they used a simplified band model, which omits all the second order far-band contributions, with the exception of a finite heavy hole mass. In order to overcome these shortcomings, we have combined the essential aspects of both approaches.[23] This enables us to calculate the optical constants based on a realistic band structure model, which includes all second order higher band contributions.

The bands of both bulk HgTe and CdTe are described by Kane's four-band model ($8\times8\mathbf{k}\cdot\mathbf{p}$) including second order remote band contributions. The envelope function method in the axial approximation is widely used to calculate the band structure of the HgTe/CdTe SL.[18,19] The axial approximation gives exact results for the band gaps of (001) oriented systems, because nonaxial terms in the Hamiltonian vanish for $\mathbf{k}_\parallel=0$. It is well known that the axial approximation is not exact for growth directions other than [001] and [111] even for $\mathbf{k}_\parallel=0$.[24] Therefore we have taken the approach of Los, Fasolino, and Catellani[25] and transformed the Hamiltonian into symmetry adapted basis functions for the [112] growth direction. We then compared the band structure using this adapted Hamiltonian with an axial approximation for the

[112] direction. The results of the axial approximation are not exact, however, they give a good approximation, within 1 or 2 meV, for the subband energies at $\mathbf{k}_{\|}=0$ as well as for an average of the subband dispersion over all $\mathbf{k}_{\|}$ directions. Consequently all absorption coefficient calculations and most intersubband transition energy calculations were carried out using this adapted Hamiltonian in the axial approximation, in order to reduce the calculation time. Moreover our band structure model is equivalent to that used by Schultz *et al.*[26] to calculate Landau levels in (112)B HgTe quantum wells.

The effects of strain due to lattice mismatch were also taken into consideration. The lattice mismatch between HgTe and its environment is less than 0.1% which results in a shift in intersubband transition energies of less than 3 meV and can therefore be neglected. In contrast to the [001] direction,[20] the strain tensor for the [112] direction has a shear strain component. This results in a piezoelectric field in the growth direction.[27] We have calculated the strain for a free standing, strained (112)B SL and a fully strained (112)B SL on a $Cd_{0.96}Zn_{0.04}Te$ substrate. From these results the piezoelectric field has been calculated to be less than 5 mV/100 Å whose influence on intersubband transition energies is less than 1 meV and can therefore be neglected in the calculations.

A revised set of values for the band parameters deduced from measurements on bulk HgTe and $Hg_{1-x}Cd_xTe$ by Weiler[28] were employed which nevertheless reproduce the same bulk band structure ($\Delta=1.0$ eV, $\gamma_1=4.1$, $\gamma_2=0.5$, $\gamma_3=1.3$, $F=0$, and $E_p=18.8$ eV):

$$m^*_{\mathrm{hh}}(112)=\left[\gamma_1-2\gamma_2-\frac{3}{2}(\gamma_3-\gamma_2)\right]^{-1}m_0=0.53m_0, \tag{2}$$

$$m^*_{\mathrm{hh}}(001)=(\gamma_1-2\gamma_2)^{-1}m_0=0.32m_0 \quad \text{at 5 K.} \tag{3}$$

The SL band structure is primarily determined by that of the quantum well and is influenced to a much lesser degree by the band structure of the barrier. Therefore the above values were employed for both the HgTe quantum wells and the $Hg_{1-x}Cd_xTe$ barriers. According to Weiler[28] the only parameter that changes significantly with alloy composition and temperature is the energy gap. The energy gaps of HgTe and $Hg_{1-x}Cd_xTe$ were taken from the empirical $E_g(x,T)$ relationship according to Laurenti *et al.*[9] with the exception of HgTe at temperatures greater than 5 K as discussed in the following sections. The valence band offset between HgTe and $Hg_{1-x}Cd_xTe$ is employed as an adjustable variable and is assumed to vary linearly with x for $Hg_{1-x}Cd_xTe$, i.e., $x\Lambda$.[29] An interface width d_t which results during growth or from interdiffusion of the two types of layers was integrated into the theory. The concentration profile across the interface is described by an error function similar to an experimental profile according to Kim *et al.*[3]

The complex dielectric constant can be written as

$$\varepsilon(\omega)=\varepsilon_R(\omega)+i\frac{\sigma(\omega)}{\omega\epsilon_0}, \tag{4}$$

where $\varepsilon_R(\omega)$ is the residual contribution of the lattice and higher subbands which is assumed to be constant over the frequencies of interest in this investigation, $\varepsilon_R(\omega)\approx 10$. The complex dynamic conductivity, $\sigma(\omega)$, is determined by making use of Kubo's formula[23] and finally the absorption coefficient is given by

$$\alpha(\omega)=\frac{\omega}{c}\frac{\sqrt{2}\varepsilon_2(\omega)}{\sqrt{\varepsilon_1(\omega)+|\varepsilon(\omega)|}}, \tag{5}$$

where $\varepsilon_1(\omega)$ and $\varepsilon_2(\omega)$ are the real and imaginary components of $\varepsilon(\omega)$, respectively.

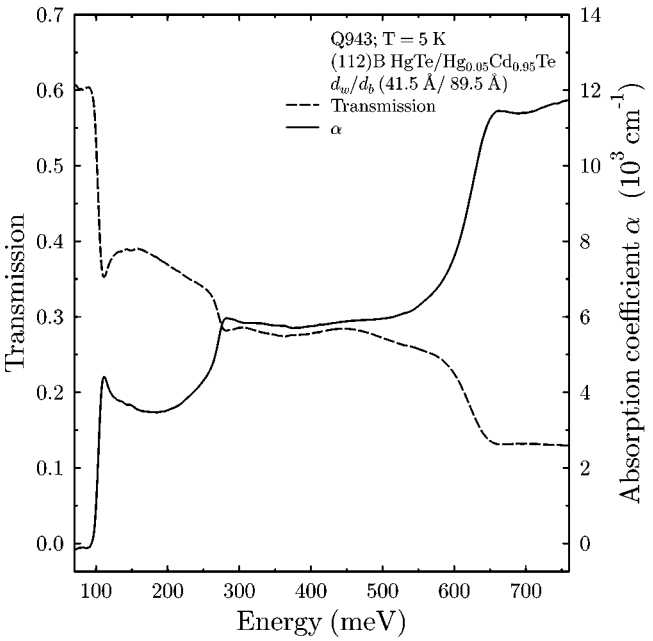

FIG. 1. Transmission and absorption spectra of the (112)B $HgTe/Hg_{0.05}Cd_{0.95}Te$ superlattice Q943 at 5 K.

IV. RESULTS AND DISCUSSION

A. (112)*B* orientation

The transmission and absorption spectra for a (112)*B* $HgTe/Hg_{0.05}Cd_{0.95}Te$ SL at 5 K are shown in Fig. 1. Three distinctive steps are observed which we have assigned to the $H1$-$E1$, $L1$-$E1$, and $H2$-$E2$ intersubband transitions. *H*, *L*, and *E* are the heavy hole, light hole, and electron subbands, respectively. In contrast, Yang *et al.*[6] attributed the first two steps at lower energies in a similar SL to the $H1$-$E1$ and $H2$-$E2$ transitions, and the weak shoulder near 240 meV to $L1$-$E1$. In order to insure a correct assignment, there must be agreement between the calculated transition probabilities and the observed absorption coefficient spectrum as well as between the calculated and experimental frequencies. That this is the case here, is demonstrated in Fig. 2 where the experimental and theoretical absorption as well as the calculated absorption for the three individual transitions are plotted versus energy. The relative heights of the three steps are in good agreement with experiment, even though their absolute magnitudes are underestimated due to the neglect of Coulomb interaction between electron and hole.[30] The energies of the $H1$-$E1$ and $L1$-$E1$ transitions are in good agreement whereas agreement is only fair at higher energies, e.g., for $H2$-$E2$, as expected for a perturbation theory. The weak

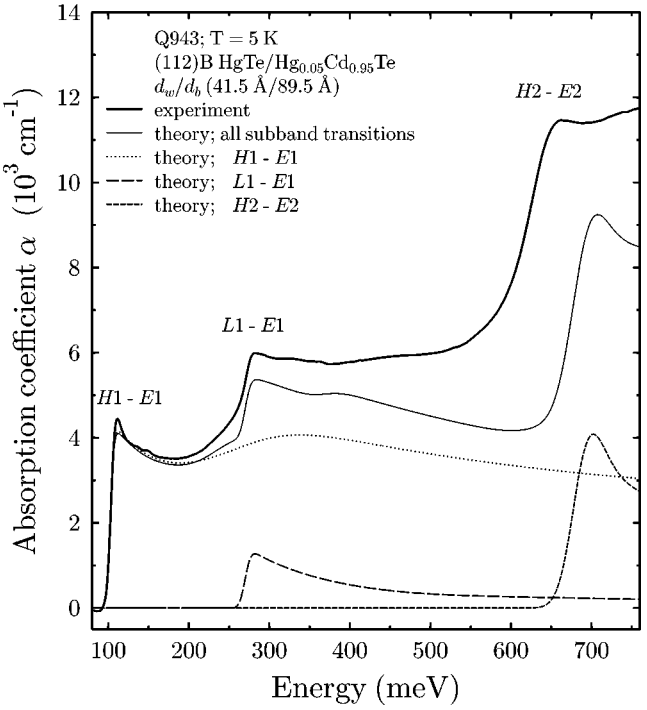

FIG. 2. Experimental and theoretical absorption coefficients of the (112)B $HgTe/Hg_{0.05}Cd_{0.95}Te$ superlattice Q943 at 5 K. Also shown are the individual contributions of the $H1$-$E1$, $L1$-$E1$, and $H2$-$E2$ intersubband transitions.

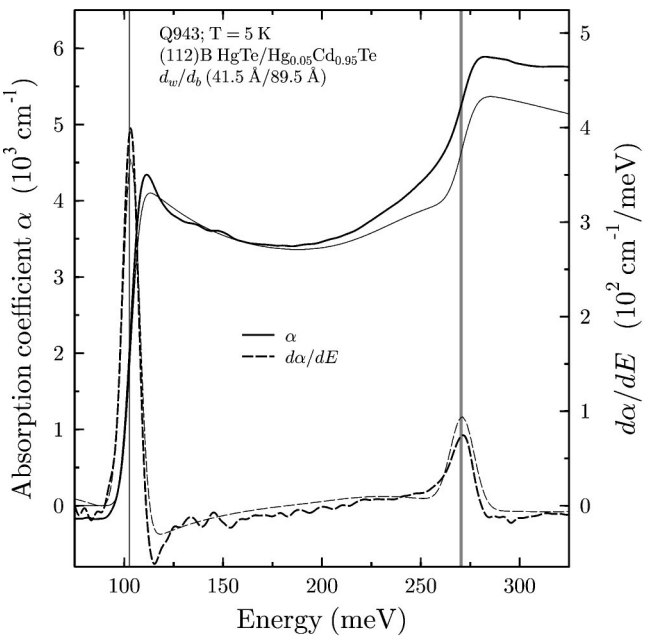

FIG. 3. Experimental (thick line) and theoretical (thin line) absorption coefficients, and their first derivatives (thick and thin dashed lines, respectively) for the (112)B $HgTe/Hg_{0.05}Cd_{0.95}Te$ SL $Q943$ at 5 K. The intersubband transition energies are indicated by vertical lines and their dispersion for $\mathbf{q}\|\mathbf{z}$, the miniband width, by the width of these vertical lines.

shoulder near 240 meV is due to the $H2$-$E1$ transition which is allowed only for $\mathbf{k}>0$. For these reasons and others which will become apparent below, we shall concentrate on the $H1$-$E1$ and $L1$-$E1$ transitions.

1. Intersubband transition energies

The absorption edges have been determined by two different methods. In the first method, the absorption edge is defined as the energy at the maximum value of the first derivative of the absorption coefficient. This is schematically demonstrated in Fig. 3 for $Q943$ at 5 K. The full widths at half maximum FWHM of the derivative for the $H1$-$E1$ and $L1$-$E1$ transitions are 8.5 and 13 meV, respectively. Also shown is a theoretically calculated α and its derivative, together with the calculated intersubband transition energies. The dispersion for these transitions is indicated by the width of the two vertical lines, i.e., $\approx$0.5 and $\approx$1.8 meV for these two transitions. A small energy dispersion and hence a wide barrier is desired in order to minimize uncertainties in the transition energies. The barrier widths of most of the SL's in this investigation are $\geqslant$80 Å, which result in a dispersion of $\leqslant$1.0 and $\leqslant$3.5 meV, respectively. The shape and width of the experimental α and $d\alpha/dE$ of $Q943$ were simulated by assuming a Gaussian distribution of quantum well widths with $\Gamma = 1.5$ Å.[31] As can be seen, the absorption edges coincide with the intersubband transition energies to within ± 1 meV. In this investigation an uncertainty of $\leqslant \pm 2$ meV holds for all samples, with one exception in which a systematic discrepency of 4 meV for $L1$-$E1$ is observed. This is due to interference effects which have not been completely removed but being known can be taken into account.

In the second method the absorption edge is determined from the change in the absorption coefficient according to Eq. (1). The near equivalence of these two methods of determining the band edges and consequently the intersubband transition energies are demonstrated in Fig. 4. In this figure the dashed line represents $d\alpha/dE$ at 40 K and the solid line represents $T_{60\,K}/T_{20\,K}-1$ whose effective temperature is 40

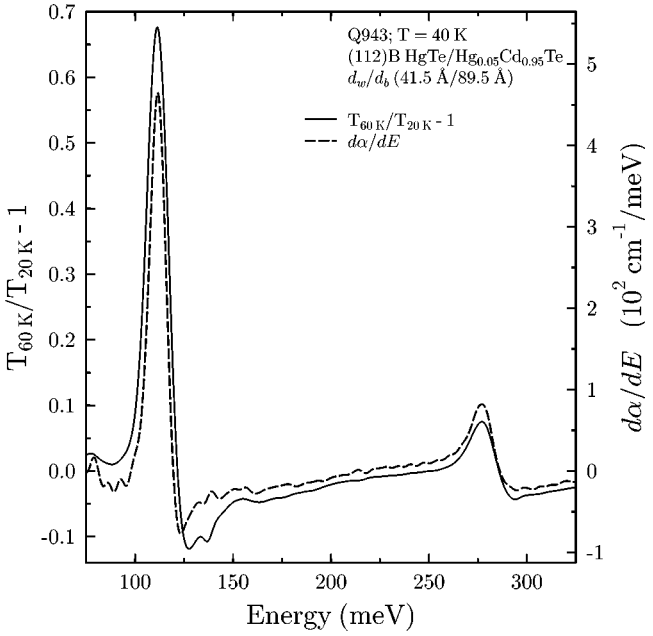

FIG. 4. Ratio of transmission T spectra at $T=60$, and $T=20$ K (solid line) is compared with the first derivative of α (dashed line) for Q943 at 40 K.

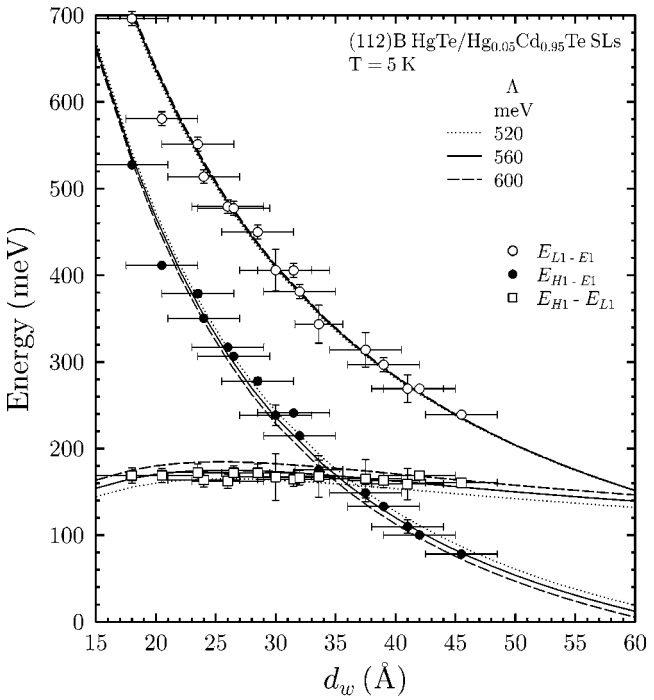

FIG. 5. Experimental values for $E_{H1\text{-}E1}$ (filled circles), $E_{L1\text{-}E1}$ (empty circles), and the energy difference $E_{H1}-E_{L1}$ (empty squares) for all (112)B SL's together with theoretical results at 5 K (lines) are plotted vs d_w. Calculated results using $d_t=24$ Å and $x_w=0.00$ for possible values of Λ are shown. d_t is the interface width.

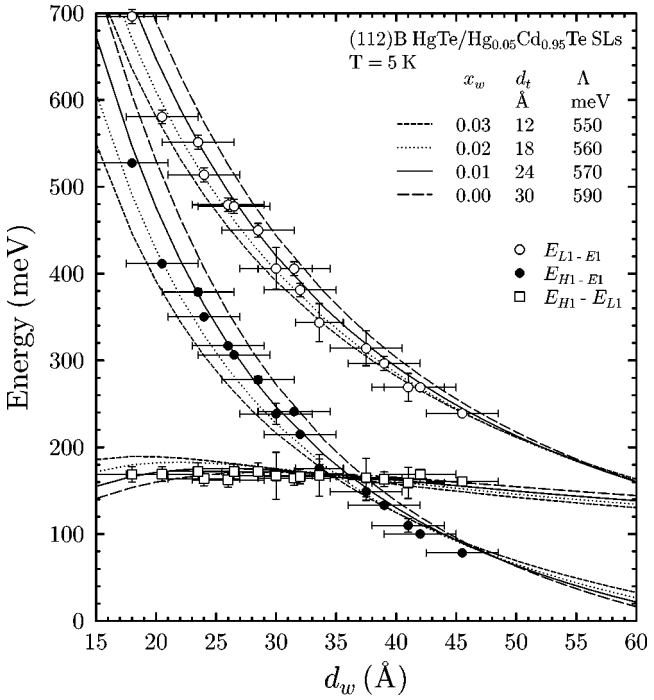

FIG. 6. Experimental values for $E_{H1\text{-}E1}$ (filled circles), $E_{L1\text{-}E1}$ (empty circles), and $E_{H1}-E_{L1}$ (empty squares) for all (112)B SL's together with theoretical results at 5 K (lines) are plotted vs d_w. Calculated results for possible values of Λ and superlattice parameters are shown.

TABLE I. Average value of the valence-band offset between HgTe and CdTe, $\overline{\Lambda}$, necessary to predict the experimental value of $E_{H1}-E_{L1}$ and its standard error for a range of all feasible superlattice parameters for the (112)B and (001) orientations at 5 K.

	d_t (Å)	x_w	$\overline{\Lambda}$ (meV)
(112)*B*	18	0.02	556±12
	24	0.00	561±7
	24	0.01	573±8
	30	0.00	590±7
(001)	18	0.03	546±9
	24	0.02	552±7
	30	0.00	552±7
	30	0.01	565±7
	36	0.00	583±8

K. The experimental transition energy defined as the energy at the maximum value of $T_{60\,K}/T_{20\,K}-1$ is in good agreement with the corresponding energy for $d\alpha/dE$, in this case the energy difference is $\leqslant 1$ meV for both transitions.

The energies of the $H1$-$E1$ and $L1$-$E1$ transitions at 5 K for all of the investigated (112)B SL's are plotted versus quantum well width, d_w, in Fig. 5. Also shown is the energy difference between these two intersubband transitions, i.e., E_{H1}-E_{L1}=$E_{L1\text{-}E1}$-$E_{H1\text{-}E1}$. Obviously both transitions have a strong inverse dependence on d_w, whereas E_{H1}-E_{L1} is nearly independent of d_w. On the other hand, E_{H1}-E_{L1} depends nearly linearly on the valence band offset Λ. Hence a determination of Λ is possible which is not influenced by uncertainties in d_w. The three sets of lines in Fig. 5 are the

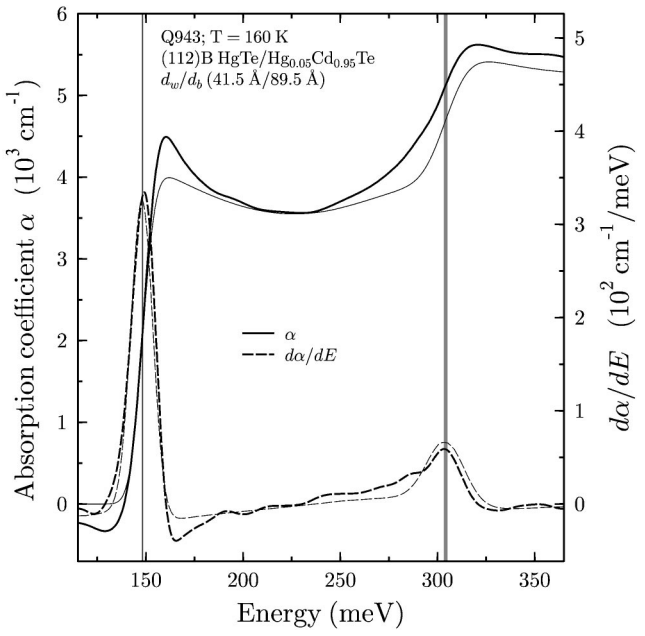

FIG. 7. Experimental (thick line) and theoretical (thin line) absorption coefficients, and their first derivatives (thick and thin dashed lines, respectively) for the (112)B HgTe/$Hg_{0.05}Cd_{0.95}$Te SL *Q*943 at 160 K. The intersubband transition energies are indicated by vertical lines and their dispersion for $\mathbf{q}\|\mathbf{z}$, the miniband width, by the width of these vertical lines.

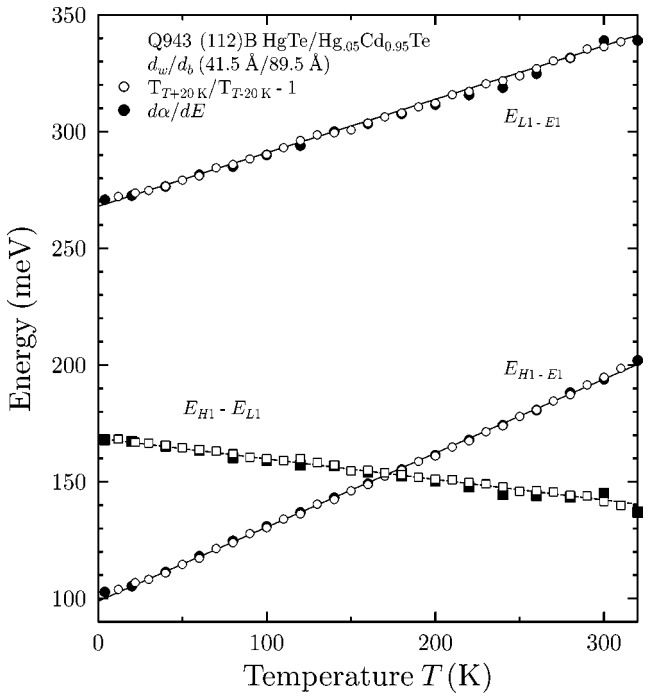

FIG. 8. Experimental $H1$-$E1$ and $L1$-$E1$ intersubband transition energies as well as $E_{H1}-E_{L1}$ are plotted as a function of temperature. Values determined from $d\alpha/dE$ are represented by filled symbols and those from the transmission ratio by empty symbols. The lines are the results of theoretical calculations using the SL parameters indicated in the figure and discussed in the text.

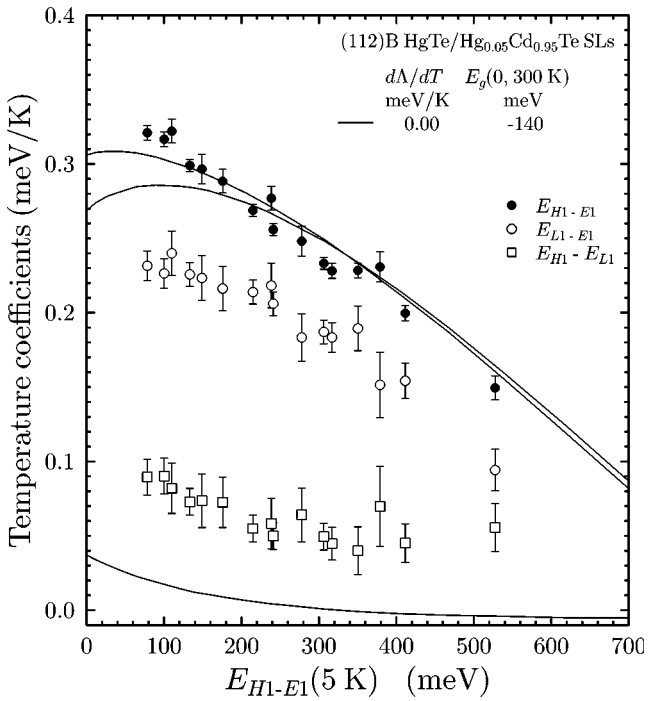

FIG. 9. Linear temperature coefficients for $E_{H1\text{-}E1}$ (filled circles), $E_{L1\text{-}E1}$ (empty circles), as well as $E_{H1}-E_{L1}$ (empty squares) are plotted vs $E_{H1\text{-}E1}$ at 5 K for all (112)B SL's. Calculated results for $d_t=24$ Å, $x_w=0.00$, $\Lambda_0=560$ meV and taking Λ to be independent of temperature, $d\Lambda/dT=0.0$ meV/K, are reproduced as solid lines.

results of the theory for these intersubband energies for a series of values for Λ assuming $d_t=24$ Å and $x_w=0.0$.

Even though the growth conditions for these SL's were as similar as possible, with the exception of the growth temperature for three SL's, a variation in SL parameters such as x_w and d_t is possible. A number of superlattice parameter sets give good to acceptable agreement with the experimental values, however, Λ is nearly independent of the set chosen. This is schematically illustrated in Fig. 6. As can be seen the experimental and calculated energies for the $H1$-$E1$ and $L1$-$E1$ intersubband transitions agree within the experimental uncertainties in these energies and in d_w. In addition the experimental values for E_{H1}-E_{L1} agree with the calculations employing the values of Λ shown in Fig. 6. The above is true for this range of superlattice parameters. SL parameters which do not fulfill this criterion have been excluded from the following statistical analysis.

Because the values of x_w and d_t and their variations are uncertain, an analysis for each feasible set of parameters has been carried out. The calculated value of Λ necessary to reproduce the experimental value of E_{H1}-E_{L1} for each of the 16 SL's has been averaged. This average value of Λ and its standard error are tabulated for each set of parameters in Table I. The Λ values for each SL have been weighted in inverse proportion to the experimental uncertainties in E_{H1}-E_{L1} shown in Figs. 5 and 6. The results may be summarized as a range of possible values at 5 K expressed as $\Lambda=570\pm26$ meV.

2. Temperature dependence

Spectra of the absorption coefficient and its derivative for $Q943$ at 160 K are reproduced in Fig. 7. The absorption edges as defined by $d\alpha/dE$ are shifted to higher energies and are slightly broader with a FWHM of 15 and 22 meV for the $H1$-$E1$ and $L1$-$E1$ intersubband transitions, respectively. However their shapes are similar to those at 5 K and the intersubband transition energies coincide with the peaks of $d\alpha/dE$ within ±2 meV. This is true up to room temperature, therefore, an accurate temperature coefficient for these transitions can be determined. The $H1$-$E1$ and $L1$-$E1$ intersubband transition energies for $Q943$ are shown as a function of temperature in Fig. 8. Values determined from the transmission ratio are indicated by empty circles and those from $d\alpha/dE$ by filled circles. The energies from these two methods are nearly equal: Most of the latter symbols are obscured by the former. As can be seen there is less scatter in the data from the transmission ratio method. A small Burstein-Moss[32] shift of about 2 meV can be seen at temperatures below 50 K.

Experimental values of E_{H1}-E_{L1}, which are plotted versus temperature as empty and filled squares, display a significant temperature dependence. Therefore according to the conclusions presented above, Λ is also temperature dependent. Linear temperature coefficients have been calculated for these three energies using the SL parameters determined below, and are displayed in Fig. 8 as three lines. Obviously, the calculated results are in excellent agreement with the experimental values. Because the temperature dependence of E_{H1}-E_{L1} is linear within experimental uncertainties, we propose that this is also the case for Λ:

$$\Lambda(T)=\Lambda_0+\frac{d\Lambda}{dT}T. \tag{6}$$

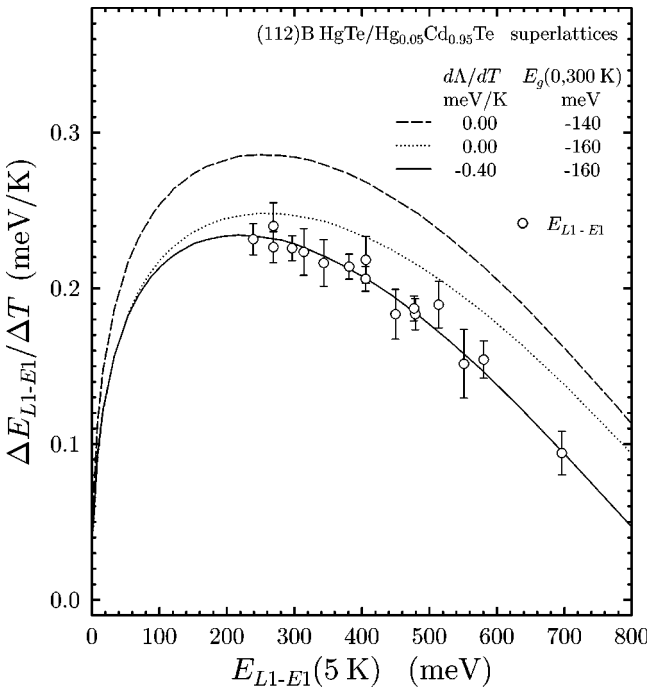

FIG. 10. Linear temperature coefficient for $E_{L1\text{-}E1}$ (empty circles) is plotted vs $E_{L1\text{-}E1}$ at 5 K for all (112)B SL's. Calculated results are shown for the following values of $E_g(0{,}300\,\mathrm{K})$ and $d\Lambda/dT$: -140 meV and 0.0 meV/K (dashed line), respectively; -160 meV and 0.0 meV/K (dotted line); -160 meV and -0.40 meV/K (solid line).

In order to determine the magnitude of this temperature dependence, we have employed a procedure which relies only on experimentally determined energies and not on d_w or other SL parameters. This is illustrated in Fig. 9 where the temperature coefficients for $E_{H1\text{-}E1}$, $E_{L1\text{-}E1}$, and E_{H1}-E_{L1} are plotted versus $E_{H1\text{-}E1}$ (5 K) for the (112)B SL's. The curves are results of the theory when Λ is assumed to be temperature independent and the energy gap of HgTe at room temperature, $E_g(0{,}300\,\mathrm{K})$, is taken to be -140 meV.[33] Even though the temperature dependence of the $H1$-$E1$ transition can be reproduced, this is clearly not the case for either $L1$-$E1$ or the energy separation between these two transitions, E_{H1}-E_{L1}. Consequently the results of previous investigations, which are based merely on the $H1$-$E1$ transition can be misleading. For example the conclusion of von Truchsess *et al.*[34] that Λ is temperature independent, is obviously incorrect.

It will be demonstrated below that the temperature dependence of the $L1$-$E1$ intersubband transition is determined by the temperature dependence of both the HgTe band gap and Λ:

$$\frac{dE_{L1\text{-}E1}}{dT} = f\left(\frac{dE_g(0,T)}{dT}, \frac{d\Lambda}{dT}\right). \tag{7}$$

The calculated temperature dependence of $E_{L1\text{-}E1}$ is compared with experiment in Fig. 10. Calculated values for $E_{L1\text{-}E1}$ approach zero for very wide quantum well widths, i.e., pure HgTe, and consequently this is also true for $\Delta E_{L1\text{-}E1}/\Delta T$. Shown in Fig. 10 are calculations assuming Λ to be independent of temperature together with both $E_g(0{,}300\,\mathrm{K}) = -140$ and -160 meV, dashed and dotted line, respectively. Decreasing this energy from -140 to -160 meV improves the fit at low energies whereas the shape at higher energies is increasingly determined by the value of $d\Lambda/dT$. A least square fit of Eq. (7) to the experimental values, shown as a solid line in Fig. 10, results in $E_g(0{,}300\,\mathrm{K}) = -160 \pm 2$ meV and $d\Lambda/dT = -0.40 \pm 0.04$ meV/K, which are listed in Table II. This value for $E_g(0{,}300\,\mathrm{K})$ differs appreciably from literature values of -140 and -120 meV,[33,9] which clearly lie outside of the experimental uncertainties in this investigation. However, these two values are not experimental values: They have been determined by extrapolating experimental results for $T < 100$ K up to room temperature. The empirical relationship for the band gap of $Hg_{1-x}Cd_xTe$ according to Laurenti *et al.*[9] has been modified as follows in order to incorporate our value for HgTe:

$$\begin{aligned} E_g(x,T) = &-303(1-x) + 1606x - 132x(1-x) \\ &+ [4.95(1-x) + 3.25x - 3.93x(1-x)] \\ &\times 10^{-1} T^2/[11(1-x) + 78.7x + T] \end{aligned} \tag{8}$$

in units of meV. This empirical equation reproduces the $E_g(x,T)$ values of Laurenti *et al.*[9] to within 2 meV for all x values and low temperatures as well as for $x > 0.6$ and temperatures up to 300 K. In particular, $E_g(1,T)$ is unchanged for CdTe.

On the basis of x-ray photoemission spectroscopy (XPS) and ultraviolet spectroscopy (UPS) Sporken *et al.*[35] concluded that the valence-band offset between CdTe and HgTe was independent of temperature between 50 K and room temperature with an uncertainty of ± 0.25 meV/K. However the valence-band offset was not determined at $\mathbf{k} = 0$: Their UPS samples were sputtered and they employed the He I and He II emission lines whose energies correspond to a position in the Brillouin zone far removed from $\mathbf{k} = \mathbf{0}$.[36]

TABLE II. Experimentally determined values together with their uncertainties for E_g (0,300 K), Λ_0, Λ (300K), $d\Lambda/dT$, and m^*_{hh} (300 K) for the (112)B and (001) orientations.

	$E_g(0{,}300\,\mathrm{K})$ (meV)	Λ_0 (meV)	Λ (300 K) (meV)	$\frac{d\Lambda}{dT}$ (meV/K)	m^*_{hh} (5 K)[a] m_0	m^*_{hh} (300 K) m_0
(112)*B*	-160 ± 2	572 ± 26	452 ± 32	-0.40 ± 0.04	0.53	0.79 ± 0.04
(001)	-157 ± 4	566 ± 27	458 ± 34	-0.41 ± 0.10	0.32	0.40 ± 0.11

[a]After Ref. 28.

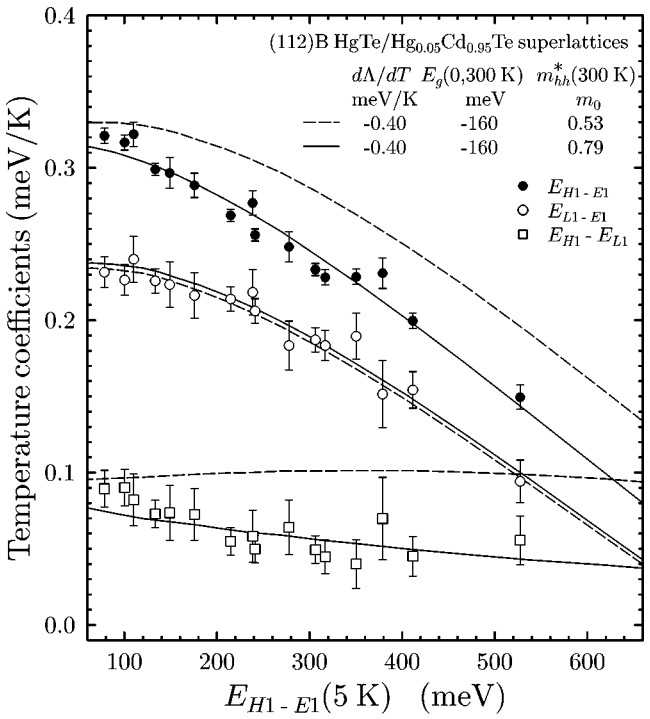

FIG. 11. Linear temperature coefficients for $E_{H1\text{-}E1}$ (filled circles), $E_{L1\text{-}E1}$ (empty circles), as well as $E_{H1}-E_{L1}$ (empty squares) are plotted vs $E_{H1\text{-}E1}$ at 5 K for all (112)B SL's. Calculated results for $d_t=24$ Å, $x_w=0.00$, $\Lambda_0=560$ meV, and $d\Lambda/dT=-0.40$ meV/K are reproduced as dashed lines, and the results when in addition $m^*_{\rm hh}$ is temperature dependent as solid lines.

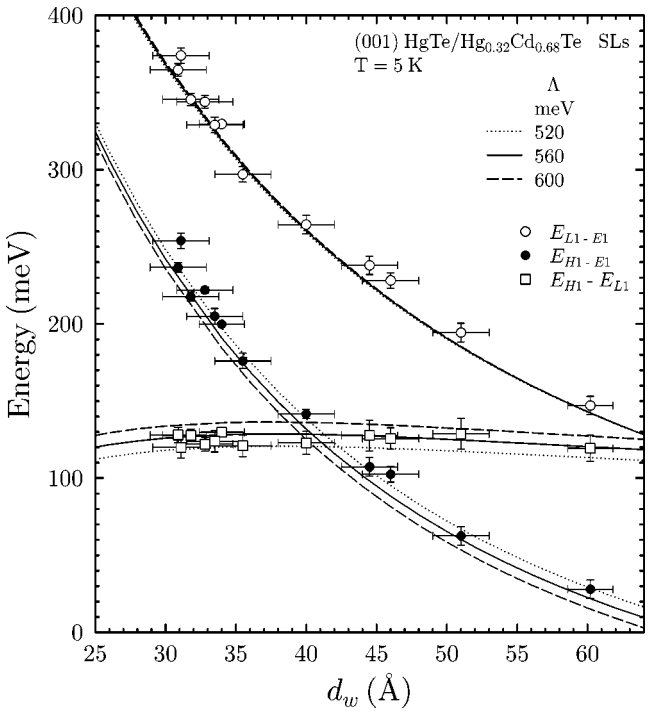

FIG. 12. Experimental values for $E_{H1\text{-}E1}$ (filled circles), $E_{L1\text{-}E1}$ (empty circles), and $E_{H1}-E_{L1}$ (empty squares) for all (001) SL's together with theoretical results at 5 K (lines) are plotted vs d_w. Calculated results using $d_t=30$ Å and $x_w=0.00$ for possible values of Λ are shown. d_t is the interface width.

The experimental temperature dependence of $E_{L1\text{-}E1}$, and that of $E_{H1\text{-}E1}$, as will be demonstrated below, cannot be explained unless Λ is temperature dependent. Since the energy gaps of HgTe and CdTe as well as either their conduction bands, valence bands, or a combination of both, depend on temperature, it would be a remarkable coincidence if the valence-band offset between the two were independent of temperature. Particularly since the band gap of HgTe increases with temperature and that of CdTe decreases.

The results for $E_{H1\text{-}E1}$, $E_{L1\text{-}E1}$, and E_{H1}-E_{L1} using a linear temperature coefficient for Λ of -0.40 meV/K are displayed in Fig. 11 by the dashed lines. Agreement with experiment at lower values of $E_{H1\text{-}E1}$ (5 K) is good as previously reported,[37] however, at higher energies this is not the case. Better agreement with experiment over the entire energy range can only be achieved by assuming that the heavy hole effective mass is also temperature dependent: One or more of the band structure parameters γ_1, γ_2, and γ_3 are temperature dependent. Analogous to the above treatment, the temperature dependence of the $H1$-$E1$ intersubband transition can be expressed as

$$\frac{dE_{H1\text{-}E1}}{dT}=f\left(\frac{dE_g(0,T)}{dT},\frac{d\Lambda}{dT},\frac{dm^*_{\rm hh}}{dT}\right). \tag{9}$$

The first two temperature coefficients have been determined above and will be held constant. A least square fit of Eq. (9) to the experimental values of $E_{H1\text{-}E1}$, which is shown as a solid line in Fig. 11 results in $m^*_{\rm hh}(112)=0.79\pm0.04\,m_0$ at 300 K, see Table II.

B. (001) orientation

This more symmetric surface has a number of advantages but also distinct disadvantages. For example, the more symmetric Hamiltonian does not lead to a monoclinic distortion or a piezoelectric effect as is the case for (112).[15,16] As mentioned above, values for the well and barrier widths via x-ray diffraction are more accurate, however, the Cd concentration in the barriers is appreciably lower, 0.68 instead of 0.95. This has two important consequences. First, due to the lower energy barrier the useful experimental data are limited to a smaller energy range. Second, the absorption edges are at least a factor of 2.5 broader, apparently due to greater alloy fluctuations in the barriers.[31]

The experimental energies for the $H1$-$E1$ and $L1$-$E1$ transitions at 5 K for all of the investigated (001) SL's are plotted versus quantum well width in Fig. 12. The energy difference between these two intersubband transitions is also shown. Both transitions display a strong inverse dependence on d_w, whereas E_{H1}-E_{L1} is nearly independent of d_w. As is the case for the (112)B SL's, E_{H1}-E_{L1} is, within experimental error, linearly dependent on the valence-band offset Λ which permits a determination of Λ independent of uncertainties in d_w. The three sets of lines in Fig. 12 are the results of the theory for these intersubband energies for a series of values for Λ assuming $d_t=30$ Å and $x_w=0.0$.

As demonstrated above for (112)B SL's, good to acceptable agreement with the experimental values of E_{H1}-E_{L1} can also be achieved for (001) SL's with a number of SL parameters, however, Λ is nearly independent of the set chosen. This is schematically illustrated in Fig. 13. The calculated value of Λ for each set of SL parameters necessary to repro-

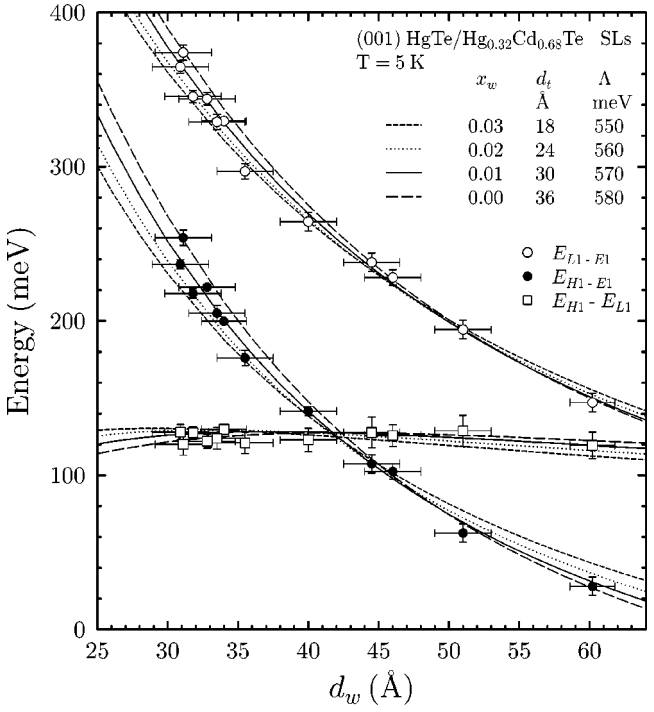

FIG. 13. Experimental values for $E_{H1\text{-}E1}$ (filled circles), $E_{L1\text{-}E1}$ (empty circles), and $E_{H1}-E_{L1}$ (empty squares) for all (001) SL's together with theoretical results at 5 K (lines) are plotted vs d_w. Calculated results for possible values of Λ and superlattice parameters are shown.

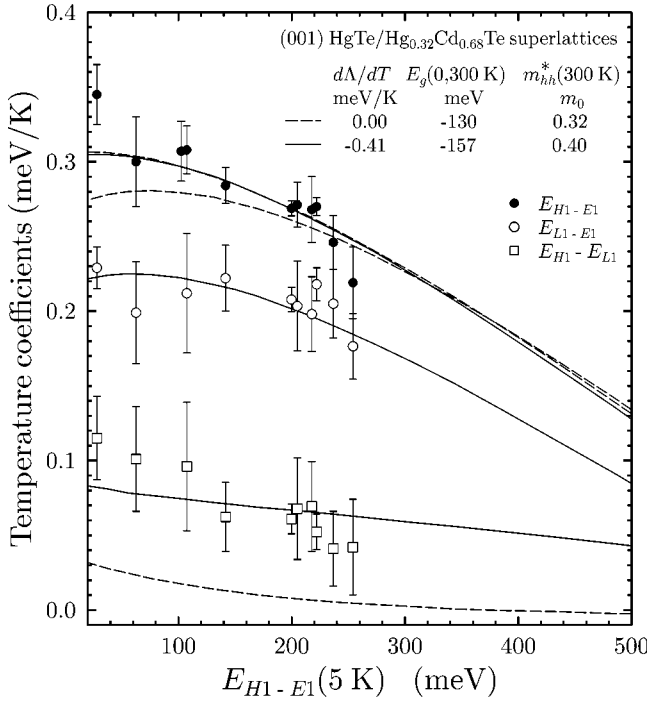

FIG. 14. Linear temperature coefficients for $E_{H1\text{-}E1}$ (filled circles), $E_{L1\text{-}E1}$ (empty circles), as well as $E_{H1}-E_{L1}$ (empty squares) are plotted vs $E_{H1\text{-}E1}$ at 5 K for all (001) SL's. Calculated results for $d_t=30$ Å, $x_w=0.00$ and $\Lambda_0=560$ meV together with the presumption that Λ and $m^*_{\rm hh}$ are independent of temperature are reproduced as dashed lines and results of a least square fit in which Λ and $m^*_{\rm hh}$ are temperature dependent as solid lines.

duce the experimental value of E_{H1}-E_{L1} for the 12 SL's has been averaged. These average values of Λ and their standard errors are tabulated for each set of parameters in Table I. The Λ values for each SL have been weighted in inverse proportion to the experimental uncertainties in E_{H1}-E_{L1} shown in Figs. 12 and 13. A range of possible values which can generate the experimental results at 5 K is given by $\Lambda=564\pm27$ meV.

The experimental linear temperature coefficients for $E_{H1\text{-}E1}$, $E_{L1\text{-}E1}$, and E_{H1}-E_{L1} together with calculations assuming a temperature-independent Λ and $E_g(0{,}300\,\mathrm{K})=-130$ meV are displayed in Fig. 14 by the dashed lines. Agreement with experiment for the temperature dependence of $E_{H1\text{-}E1}$ is reasonable, however, that is obviously not the case for either $E_{L1\text{-}E1}$ or $E_{H1}-E_{L1}$. A least square fit of $E_{L1\text{-}E1}$ to the calculated relationship of Eq. (7) and that of $E_{H1\text{-}E1}$ to Eq. (9), which is shown in Fig. 14 as solid lines, results in $d\Lambda/dT=-0.41\pm0.10$ meV/K, $E_g(0{,}300\,\mathrm{K})=-157\pm4$ meV, and $m^*_{\rm hh}(001)=0.40\pm0.11\,m_0$ at 300 K, as listed in Table II.

C. $E_g(0{,}300\,\mathrm{K})$, $\Lambda(T)$, and $m^*_{\rm hh}(T)$

The valence-band offset between HgTe and CdTe, Λ, has been the subject of a long standing controversy, which has been reviewed by, for example, Meyer *et al.*[38] In early magneto-optical experiments on semiconducting superlattices, both a small offset of 40 meV and a larger value of approximately 350 meV were deduced.[39,12] In contrast, x-ray and ultraviolet photoelectron spectroscopy have provided a consistent value of approximately 350 meV.[40,35,29] Johnson, Hui, and Ehrenreich[41] resolved the apparent controversy in favor of the larger Λ, demonstrating that with increasing Λ, HgTe/CdTe superlattices would change from semiconducting behavior to semimetallic and back to semiconducting behavior due to crossing and uncrossing of the $H1$ and $E1$ subbands. The authors showed that the electron cyclotron mass observed in previous magneto-optical experiments[39] could be explained better with 350 meV as opposed to 40 meV. The most widely accepted value has been 350 meV from XPS and UPS measurements, however, values for Λ up to 800 meV have been subsequently reported for magneto-optical experiments.[42] An offset of 550 meV at liquid helium temperatures have been deduced from photoluminescence and magneto-optical spectra, however, this value is the offset between HgTe and $Hg_{0.15}Cd_{0.85}Te$ which scales linearly to about 650 meV between HgTe and CdTe.[6] A magneto-optical investigation of the electron effective mass at the conduction band edge together with the energy of all four observed intersubband transitions for a (001) SL by von Truchsess *et al.*[10] resulted in a value of 550 ± 50 meV at 4.2 K. From the crossing of a Landau level from the conduction subband with one from the valence subband in an (112)B HgTe/CdTe quantum well with inverted band structure, Schultz *et al.*[26] obtained a value of 610 meV for Λ.

In the present investigation we have demonstrated that $\Lambda=570\pm30$ meV at 5 K for both the (001) and the (112)B orientation, by taking advantage of the fact that the valence band offset between HgTe and CdTe is primarily responsible for the separation between the $H1$-$E1$ and $L1$-$E1$ transition energies of $HgTe/Hg_{1-x}Cd_xTe$ superlattices with a normal band structure. Values for either $E_{H1\text{-}E1}$ or $E_{L1\text{-}E1}$ can be

simulated by varying one or more of the many superlattice parameters, however, to a good approximation, all relevant superlattice parameters have little or no effect on this energy difference, with the exception of Λ. This leads to an unambiguous value or range of values for Λ. This range of possible values, ± 30 meV, is due to a weak dependence on other superlattice parameters x_w and d_t and uncertainties in their values. According to Wood and Zunger[22] the accuracy of subband energies near the Γ point for the $\mathbf{k}\cdot\mathbf{p}$ method in the envelope function approximation primarily reflects the accuracy of the $\mathbf{k}\cdot\mathbf{p}$ band parameters for the bulk constituents, weighted by the magnitude of their presence in the superlattice. Consideration of the experimental uncertainties in the parameters for the bulk constituents[28] as well as the uncertainties in the superlattice parameters discussed above, result in $\Lambda = 570 \pm 60$ meV for (001) and (112)B at 5 K.

In most UPS investigations[35] Λ was not determined at $\mathbf{k} = \mathbf{0}$ and XPS experiments average over all $\mathbf{k}$ values. Dispersion in $\mathbf{k}$ space is quite different in HgTe and CdTe, and the extrapolation method of determining the valence band maximum can be less accurate for $\mathbf{k} \neq \mathbf{0}$.[36] In spite of the possibility of large systematic errors due to these facts, a value of $\approx$350 meV at 300 K has been consistently obtained. The study of Eich *et al.*[36] at $\mathbf{k} \approx 0$ is a notable exception which reports a value of 530 ± 30 meV at 300 K. The room temperature value determined here, 450 ± 60 meV, lies between these two values.

The temperature dependence of both $H1$-$E1$ and $L1$-$E1$ intersubband transitions can only be explained, if $E_g(0{,}300\,\mathrm{K}) = -160 \pm 5$ meV and if both Λ and m^*_{hh} have a significant temperature dependence. This requisite dependence in both cases can be expressed as a linear dependence. In the former case, $d\Lambda/dT = -0.40 \pm 0.04$ meV/K for $(112)B$ and, even though there is no *a priori* reason that Λ and its temperature coefficient must be equivalent for these two orientations, within experimental error, this is the case, i.e., $d\Lambda/dT = -0.41 \pm 0.10$ meV/K for (001). Sporken *et al.*[35] concluded from an XPS and UPS study that the valence-band offset between HgTe and CdTe was independent of temperature between 50 K and room temperature with an uncertainty of ± 0.25 meV/K. However, the authors did not determine the valence-band offset at $\mathbf{k} = \mathbf{0}$, which can lead to large systematic errors according to the arguments given above. In the latter case, $m^*_{\mathrm{hh}}(112) = 0.79 \pm 0.04\, m_0$ at 300 K when the literature value[28] of $m^*_{\mathrm{hh}}(112) = 0.53\, m_0$ at 5 K is employed, and $m^*_{\mathrm{hh}}(001) = 0.40 \pm 0.11\, m_0$ at 300 K compared to the value employed at 5 K, $m^*_{\mathrm{hh}}(001) = 0.32\, m_0$,[28] see Table II. If these values for $m^*_{\mathrm{hh}}(001)$ according to Eq. (3) are inserted into Eq. (2) then the resulting anisotropic component of $m^*_{\mathrm{hh}}(112)$, i.e., $(\gamma_3 - \gamma_2)$, is temperature independent, within experimental uncertainty.

The resulting temperature coefficients for $H1$-$E1$ and $L1$-$E1$ are in good agreement with experiment as can be seen in Figs. 11 and 14. Meyer *et al.*[7] have determined the temperature coefficient of the photoluminescence peak for several (112)B HgTe/$Hg_{0.10}Cd_{0.90}$Te SL's. These values are also in reasonably good agreement with our model within the uncertainty in the position of the peak relative to the $H1$-$E1$ intersubband transition energy.[43]

The band gap of HgTe has been determined by conventional magneto-optical methods only for temperatures up to approximately 100 K.[1] These values have been combined with $Hg_{1-x}Cd_xTe$ band gap energies for $x \geqslant 0.23$ and temperatures up to room temperature in empirical relationships,[33,9] which extrapolate to values for $E_g(0{,}300\,\mathrm{K})$ of -140 and -120 meV, respectively. These values are significantly larger than the experimentally determined value in this investigation, i.e., $E_g(0{,}300\,\mathrm{K}) = -160 \pm 5$ meV.

V. CONCLUSIONS

Intersubband transitions and their dependence on temperature in semiconducting HgTe/$Hg_{1-x}Cd_xTe$ superlattices with normal band structure have been investigated for a large number of superlattices. It has been demonstrated that Λ is primarily responsible for the separation between the $H1$-$E1$ and $L1$-$E1$ transition energies of HgTe/$Hg_{1-x}Cd_xTe$ superlattices with normal band structure. To a good approximation, all other relevant superlattice parameters have little or no effect on this energy difference. This leads to a value for the valence band offset between HgTe and CdTe given by $\Lambda = 570 \pm 60$ meV at 5 K for both the (001) and the $(112)B$ orientations. This uncertainty in Λ is due to uncertainties in the $\mathbf{k}\cdot\mathbf{p}$ band parameters of the bulk constituents as well as due to a weak dependence on x_w and d_t and uncertainties in their values.

An explanation of the temperature dependence for both of these intersubband transition energies leads to the following unambiguous conclusions. Λ is temperature dependent as described by the linear temperature coefficient of -0.40 ± 0.04 and -0.41 ± 0.10 meV/K for (112)B and (001), respectively. Within experimental error, these values are equivalent. Thus $\Lambda = 450 \pm 60$ meV at 300 K for both orientations. Second, the energy gap of HgTe at 300 K is given by $E_g(0{,}300\,\mathrm{K}) = -160 \pm 5$ meV. This value is appreciably lower than the extrapolated values found in the literature. Finally the anisotropic heavy hole effective mass for HgTe was shown to have a significant temperature dependence, however, the anisotropic component of $m^*_{\mathrm{hh}}(112)$ is, within experimental uncertainty, independent of temperature.

ACKNOWLEDGMENT

The support of the Deutsche Forschungsgemeinschaft via SFB 410, II-VI *Halbleiter: -Wachstumsmechanismen, niederdimensionale Strukturen, und Grenzflächen,* is gratefully acknowledged.

*Email: becker@physik.uni-wuerzburg.de

[1] M. Dobrowolska, A. Mycielski, and W. Dobrowolski, Solid State Commun. **27**, 1233 (1978).

[2] V. Latussek, C. R. Becker, G. Landwehr, R. Bini, and L. Ulivi (unpublished).

[3] Y. Kim, A. Ourmazd, M. Bode, and R. D. Feldman, Phys. Rev. Lett. **63**, 636 (1989).

[4] C. R. Becker, V. Latussek, W. Spahn, F. Goschenhofer, S. Oehling, and G. Landwehr, Proc. SPIE **2554**, 6 (1995).

[5] K. A. Harris, R. W. Yanka, L. M. Mohnkern, A. R. Riesinger, T.

H. Myers, Z. Yang, Z. Yu, S. Hwang, and J. F. Schetzina, J. Vac. Sci. Technol. B **10**, 1574 (1992).
[6] Z. Yang, Z. Yu, Y. Lansari, S. Hwang, J. W. Cook, Jr., and J. F. Schetzina, Phys. Rev. B **49**, 8096 (1994).
[7] J. R. Meyer, A. R. Reisinger, K. A. Harris, R. W. Yanka, L. M. Mohnkern, and L. R. Ram-Mohan, J. Cryst. Growth **138**, 981 (1994).
[8] C. L. Cesar, M. N. Islam, R. D. Feldman, R. F. Austin, D. S. Chemla, L. C. West, and A. E. DeGiovanni, Appl. Phys. Lett. **56**, 283 (1990).
[9] J. P. Laurenti, J. Camassel, A. Bouhemadou, B. Toulouse, R. Legros, and A. Lusson, J. Appl. Phys. **67**, 6454 (1990).
[10] M. von Truchsess, V. Latussek, F. Goschenhofer, C. R. Becker, G. Landwehr, E. Batke, R. Sizmann, and P. Helgesen, Phys. Rev. B **51**, 17 618 (1995).
[11] A. Tardot, A. Hamoudi, N. Magnea, P. Gentile, and J. L. Pautrat, Appl. Phys. Lett. **62**, 2548 (1993).
[12] J. N. Schulman, O. K. Wu, E. A. Patten, Jeong W. Han, Y. Lansari, L. S. Kim, J. W. Cook, Jr., and J. F. Schetzina, Appl. Phys. Lett. **53**, 2420 (1988).
[13] M. Möller, R. N. Bicknell-Tassius, and G. Landwehr, J. Appl. Phys. **72**, 5108 (1992).
[14] C. R. Becker, L. He, M. M. Regnet, M. M. Kraus, Y. S. Wu, G. Landwehr, X. F. Zhang, and H. Zhang, J. Appl. Phys. **74**, 2486 (1993).
[15] M. Li, C. R. Becker, R. Gall, W. Faschinger, and G. Landwehr, Appl. Phys. Lett. **71**, 1822 (1997).
[16] M. Li, R. Gall, C. R. Becker, T. Gerhard, W. Faschinger, and G. Landwehr, J. Appl. Phys. **82**, 4860 (1997).
[17] D. Fasold, K. Heil, and S. Jetschke, Phys. Status Solidi A **86**, 125 (1984).
[18] L. R. Ram-Mohan, K. H. Yoo, and R. L. Aggarwal, Phys. Rev. B **38**, 6151 (1988).
[19] N. F. Johnson, H. Ehrenreich, P. M. Hui, and P. M. Young, Phys. Rev. B **41**, 3655 (1990).
[20] A. Simon, D. Bertho, D. Boiron, and C. Jouanin, Phys. Rev. B **42**, 5221 (1990).
[21] J. R. Meyer, C. A. Hoffman, and F. J. Bartoli, Semicond. Sci. Technol. **5**, S90 (1990).
[22] D. M. Wood and Alex Zunger, Phys. Rev. B **53**, 7949 (1996).
[23] E. Bangert, P. Boege, V. Latussek, and G. Landwehr, Semicond. Sci. Technol. **8**, S99 (1993).
[24] R. Winkler and A. I. Nesvizhskii, Phys. Rev. B **53**, 9984 (1996).
[25] J. Los, A. Fasolino, and A. Catellani, Phys. Rev. B **53**, 4630 (1996).
[26] M. Schultz, U. Merkt, A. Sonntag, U. Rössler, R. Winkler, T. Colin, P. Helgesen, T. Skauli, and S. Løvold, Phys. Rev. B **57**, 14 772 (1998).
[27] Liberato De Caro and Leander Tapfer, Phys. Rev. B **51**, 4374 (1995).
[28] M. H. Weiler, in *Semiconductors and Semimetals*, edited by R. Willardson and A. C. Beer (Academic, New York, 1981), Vol. 16, p. 119.
[29] C. K. Shih and W. E. Spicer, Phys. Rev. Lett. **58**, 2594 (1987).
[30] Christian Tanguy, Phys. Rev. Lett. **75**, 4090 (1995), and references therein.
[31] C. R. Becker, A. Pfeuffer-Jeschke, V. Latussek, M. Li, K. Ortner, V. Daumer, S. Oehling, W. Tang, and G. Landwehr, J. Cryst. Growth **184/185**, 1185 (1998).
[32] E. Burstein, Phys. Rev. **93**, 632 (1954); T. S. Moss, Proc. Phys. Soc. London, Sect. B **76**, 775 (1954).
[33] G. L. Hansen, J. L. Schmit, and T. N. Casselman, J. Appl. Phys. **53**, 7099 (1982).
[34] M. von Truchsess, V. Latussek, C. R. Becker, and E. Batke, J. Cryst. Growth **159**, 1128 (1996).
[35] R. Sporken, S. Sivananthan, J. P. Faurie, D. H. Ehlers, J. Fraxedas, L. Ley, J. J. Pireaux, and R. Caudano, J. Vac. Sci. Technol. A **7**, 427 (1989).
[36] D. Eich, K. Ortner, U. Groh, Z. N. Chen, C. R. Becker, G. Landwehr, R. Fink, and E. Umbach, Phys. Status Solidi A **173**, 261 (1999).
[37] C. R. Becker, V. Latussek, M. Li, A. Pfeuffer-Jeschke, and G. Landwehr, J. Electron. Mater. **28**, 826 (1999).
[38] J. R. Meyer, C. A. Hoffman, T. H. Myers, and N. C. Giles, in *Handbook on Semiconductors*, edited by S. Mahajan (North-Holland, Amsterdam, 1994), Vol. 3, p. 535.
[39] Y. Guldner, G. Bastard, J. P. Vieren, M. Voos, J. P. Faurie, and A. Million, Phys. Rev. Lett. **51**, 907 (1983); J. M. Berroir, Y. Guldner, J. P. Vieren, M. Voos, and J. P. Faurie, Phys. Rev. B **34**, 891 (1986).
[40] Steven P. Kowalczyk, J. T. Cheung, E. A. Kraut, and R. W. Grant, Phys. Rev. Lett. **56**, 1605 (1986).
[41] N. F. Johnson, P. M. Hui, and H. Ehrenreich, Phys. Rev. Lett. **61**, 1993 (1988).
[42] K. H. Yoo, R. L. Aggarwal, L. R. Ram-Mohan, and O. K. Wu, J. Vac. Sci. Technol. A **8**, 1194 (1990).
[43] Agreement is good if the photoluminescence peak E_p is shifted according to Eq. (1) in Ref. 7: $E_p = E_{H1\text{-}E1} + \upsilon k_B T$ with $\upsilon \approx 0.5$.